

TRANSIENT FLOW IN NATURALLY FRACTURED RESERVOIRS AND ITS APPLICATION TO DEVONIAN GAS SHALES

by Fikri Kucuk*, Science Applications, Inc.;
Walter K. Sawyer, West Virginia U.

*now with Sohio Petroleum Co.

This paper was presented at the 55th Annual Fall Technical Conference and Exhibition of the Society of Petroleum Engineers of AIME, held in Dallas, Texas, September 21-24, 1980. The material is subject to correction by the author. Permission to copy is restricted to an abstract of not more than 300 words. Write: 6200 N. Central Expwy., Dallas, Texas 75206.

ABSTRACT

For many years gas has been produced naturally from Devonian shales throughout the Appalachian Basin at rates which made them commercially feasible. In 1975, because of the deteriorating gas supply situation in the United States and increasing demand for energy, the U.S. Department of Energy (DOE) established the Eastern Gas Shales Project (EGSP) as part of the Unconventional Gas Recovery (UGR) program to study and characterize and to develop economically feasible technology for further exploitation of Devonian shale gas reservoirs.

Devonian shale gas reservoirs typically are characterized by a low storage, high flow-capacity natural fracture system fed by a high storage, low flow-capacity rock matrix. In this study analytical solutions are developed to analyze the basic fractured reservoir parameters that control well productivity. These parameters include fracture system porosity and permeability, matrix porosity and permeability, and matrix size.

It is shown that the conventional well test method does not usually work for fractured Devonian shale gas reservoirs. For most cases, the semilog plot of the drawdown and buildup data does not show two parallel straight lines with a vertical separation.

Numerical solutions are also used to include the Klinkenberg effect and desorption in the shale matrix.

INTRODUCTION

Fractured reservoirs have been studied for several decades. However, during the last three decades, most reservoir engineering studies have been directed toward homogeneous formations. The earliest discussion of fractured reservoir performance was the analysis of the Spraberry Field in West Texas.¹

In 1959, Pollard² presented a method to determine fracture volume from pressure buildup data. The Pollard method was extended by Pirson and Pirson³ to

References and illustrations at end of paper.

calculate the matrix volume of a fractured reservoir.

One of the classic papers on fractured reservoirs by Warren and Root⁴ considered a dual porosity system which consisted of a fractured porous medium in which matrix blocks acted as a uniformly distributed source. Natural fractures are replaced by equivalent sets of horizontal and vertical fractures. Warren and Root presented an approximate analytical solution for naturally fractured reservoirs based on the Barenblatt and Zheltov formulation.⁵ They showed that the semilog plot of pressure drawdown or buildup data for an infinite reservoir displaces two parallel straight lines whose slopes are related to the flow capacity of the formation. The vertical separation of these straight lines is related to the relative storage capacity of the fractures. Warren and Root also showed that the Pollard² and Pirson and Pirson³ techniques could lead to erroneous results in some cases.

Odeh⁶ presented a model similar to that of Warren and Root⁴. His results did not displace two parallel straight lines. He concluded that fractured reservoirs cannot be distinguished from homogeneous ones.

Later, Kazemi⁷ presented numerical solutions for fractured reservoirs. The Kazemi model consisted of a set of uniformly spaced horizontal matrix layers separated by fractures. This model can be considered a special case of the Warren and Root model. Kazemi did not use the Warren and Root assumption (i.e., that flow in the matrix blocks is quasi-steady state).

Kazemi, et al.⁸ studied the pressure behavior of an observation well in a naturally fractured reservoir with an adjacent well producing at a constant rate. This study showed that the early time response was substantially different from that of an equivalent homogeneous reservoir.

Crawford, et al.⁹ analyzed more than 20 field-measured pressure buildup curves in a reservoir known to be naturally fractured and concluded that the Warren and Root model adequately described the buildup response and is, therefore, useful in determining effective fracture permeability.

In 1976, Strobel, et al.¹⁰ demonstrated that both fracture system permeability and fracture system porosity can be obtained from type-curve analysis of pressure buildup, interference, and pulse tests in a naturally fractured dry gas reservoir.

In 1976, de Swaan¹¹ presented analytical solutions for the Warren and Root and Kazemi models by treating the matrix blocks as a source term for the fracture medium. He used the convolution theorem which yields a relationship between the source term and the pressure in the fracture medium, and introduced new variables (diffusivities) which can be used to characterize fractured reservoirs.

Later, Najurieta¹² presented an approximate solution for the de Swaan model and showed that the behavior of a uniformly fractured reservoir can be fully described by four parameters, each of which is a function of two or more of the five basic reservoir parameters (fracture and matrix porosity, fracture and matrix permeability, and fracture spacing). More recently, Najurieta¹³ applied his solutions to interference testing in naturally fractured reservoirs when boundary effects are present.

The purpose of this paper is to present a mathematical model for Devonian shale gas reservoirs which are believed to be naturally fractured. Using the model presented, we will further investigate the behavior of such reservoirs, including the Klinkenberg effect in the tight shale matrix and the effect of desorption from pore surfaces of the shale matrix.

MATHEMATICAL MODEL

Most Devonian shale gas reservoirs are believed to consist of very tight porous shale formations which contain a network of randomly distributed natural fractures. Under these conditions, the fractures may provide most of the permeability for gas flow but contribute very little to the overall storage capacity. By comparison, the matrix of the shale may provide most of the storage capacity of the shale, but has very low permeability.

Gas transport in the Devonian shale matrix can be by three primary mechanisms: Fickian diffusion, Knudsen diffusion, or Darcy flow--depending upon the pore diameter, the mean free path of the free gas molecules, and the existence of a pressure gradient.

Surface diffusion of an adsorbed gas phase may also contribute to the overall gas transport. As a matter of fact, those gases which are adsorbed on pore walls may move more efficiently than free gas molecules.

Fractured Devonian shale reservoirs are highly complex systems. Therefore, a model of an idealized fractured reservoir will be defined. This idealization is shown in Figure 1 and is similar to the Warren and Root⁴ and Kazemi⁷ models. The mathematical formulation will be the same for both models. However, the approximation for the matrix block will be a cylindrical element for model I and a spherical element for Model II.

It is assumed that gas transport in Devonian shale reservoirs occurs only in a porous fracture system into which matrix blocks of contrasting physical properties deliver their gas contents. That is, the matrix acts as a uniformly distributed gas source in a fracture medium.¹¹ Gas desorption from pore walls

will be treated as a uniformly distributed source within the matrix blocks.

Gas flow through the fractured Devonian Shale system is presented by Kucuk and Sawyer as

$$\nabla \cdot \left[\rho \frac{k_f}{\mu} \nabla p_f \right] + w_m(p_f, t) = \frac{\partial}{\partial t} (\phi_f \rho) \quad (1)$$

where

- ρ = density, g/cm³
- k_f = fracture permeability, darcy
- μ = viscosity, cp
- ϕ_f = fracture porosity
- p_f = fracture pressure, atm
- t = time, sec
- w_m = mass flow rate per volume of shale matrix element, g/sec/cm³

The equation of state for real gas is given by

$$\rho = \frac{M}{RT} \frac{p_f}{z} \quad (2)$$

Substitution of Eq. 2 into Eq. 1 yields

$$\nabla \cdot \left[\frac{k_f}{\mu} \frac{p_f}{z} \nabla p_f \right] + \frac{RT}{M} w_m(p_f, t) = \frac{\partial}{\partial t} \left(\phi_f \frac{p_f}{z} \right) \quad (3)$$

where

$$w_m(p_f, t) = - \frac{\rho_m A_m k_m}{V_m \mu} \left(\frac{\partial p_m}{\partial n} \right)_{\text{surface}}$$

- A_m = surface area of matrix element, cm²
- V_m = volume of element, cm³
- k_m = matrix permeability, darcy
- ρ_m = matrix gas density, g/cm³
- p_m = matrix pressure, atm
- n = normal to the surface of the matrix element

It is assumed that the surface pressure of the matrix element is equal to the pressure in the fracture system; i.e., p_m (matrix pressure) = p_f (fracture pressure) at the external boundary of the matrix element which assures pressure continuity at the boundary.

Equation 3 describes gas flow through the fractured shale reservoir with a source term which is the contribution from the shale matrix. Gas transport through the matrix is also described by the diffusivity equation with a source term due to desorption of gas from the pore walls of the matrix. The following equation describes the motion of gas through the matrix.

$$\nabla \cdot \left[\rho_m \frac{k_m}{\mu} \nabla p_m \right] + w_d = \frac{\partial}{\partial t} (\phi_m \rho_m) \quad (4)$$

where

- k_m = matrix permeability to gas, darcy
- w_d = desorption rate, g/sec/cm³ shale
- p_m = matrix pressure, atm
- ϕ_m = matrix porosity

The rate of desorption can be expressed as

$$w_d = -M \left(\frac{dc_d}{dp_m} \right) \frac{\partial p_m}{\partial t} \quad (5)$$

where

c_d = concentration of gas at the surface of pore walls, mole/cm³ shale

The term, $\left(\frac{dc_d}{dp_m} \right)$ in Eq. 5 is the slope of the desorption isotherm curve for a given gas and shale sample. For example, Figure 1 presents the adsorption isotherm for three shale samples from the Illinois¹⁵ Basin. The slopes of these curves can be used to determine $\frac{dc_d}{dp_m}$.

It is believed that there is a difference between the adsorption and desorption curves.

The gas permeability of a porous medium usually exceeds the liquid permeability of the same medium. The difference in these permeabilities is due to the phenomenon known as gas slippage, which is related to the mean free path of the gas molecules relative to pore diameter. Consequently, the gas permeability of a porous medium should be a function of the temperature, pressure, and the nature of the gas. Klinkenberg¹⁶ developed the relationship between gas permeability of a porous medium to a nonreactive liquid

$$k_g = k_l \left(1 + \frac{b}{p_m} \right) \quad (6)$$

where b is the Klinkenberg factor, which is constant for a given gas and a given porous medium at a constant temperature. A graph of k_g versus $1/p_m$ should result in a straight line with an intercept of k_l and a slope of bk_l . Thus, gas permeability is greater at low pressures. The Klinkenberg factor, b , was recently given by Jones and Owens¹⁷ as

$$b = 12.64 k_l^{-.33} \quad (7)$$

for gas sands in the permeability range of 0.1 md to .0001 md.

Since pore diameters are small for Devonian shales, b is expected to be large. Therefore, the Klinkenberg effect or slippage factor cannot be ignored in the Devonian shale model.

Substitution of Equations 2, 5, and 6 into Eq. 4 yields

$$\nabla \left[\frac{k_l p_m}{\mu} \left(1 + \frac{b}{p_m} \right) \nabla p_m \right] = \phi_d \left(\frac{\partial p_m}{\partial t} \right) + \phi_m \frac{\partial}{\partial t} \left(\frac{p_m}{z} \right) \quad (8)$$

where $\phi_d = \left(\frac{dc_d}{dp_m} \right) RT$, dimensionless

The source term in Eq. 3 can be determined from the solution of Eq. 8. An iterative finite-difference solution technique is used to solve Equations 3 and 8 simultaneously. The numerical treatment of the above

equations has been discussed in detail in Ref. 14. In this study, both analytical and numerical solutions will be used to predict the pressure and rate behavior of a Devonian shale gas well. A description of an analytical method of solving the idealized fractured flow system is given below.

ANALYTICAL SOLUTIONS

At the most fundamental level, analytic solutions of idealized flow systems help to provide a better understanding of the basic flow phenomena. They may also be used to explore, in a very general and qualitative manner, the sensitivity of modeling predictions to a variety of different effects. Another useful class of analytic solutions to the flow equations arises in connection with the interpretation of well test flow data which are taken in order to learn about the local *in situ* reservoir properties.

The following simplifying assumptions have been made in the development of the analytical solutions.

1. An isotropic infinite reservoir of uniform thickness, h .
2. All formation properties independent of pressure.
3. No Klinkenberg effect.
4. No desorption within matrix elements.
5. Matrix elements consist of cylinders with radius a and height h which are equal to the formation thickness, or spheres with radius a .

For simplicity, pressure will be used as a dependent variable. Pressure squared or pseudo-pressure can also be used for a more rigorous treatment of the gas flow as in Ref. 14. Solutions for finite difference systems are also presented in Ref. 14.

Two conditions at the wellbore are of paramount importance in reservoir studies; namely, the constant-pressure and the constant-rate cases. In this analytical treatment, it is assumed that the well is producing at a constant rate. Under these conditions, Eq. 3 can be written in radial-cylindrical coordinates as

$$\frac{1}{r} \frac{\partial}{\partial r} \left(r \frac{\partial p_f}{\partial r} \right) - \frac{\mu}{k_f} q_m \left(p_f, t \right) = \frac{1}{\eta_f} \left(\frac{\partial p_f}{\partial t} \right) \quad (9)$$

where

$$\eta_f = \frac{k_f}{\phi_f \mu c_t}$$

$$\Delta p_f = p_i - p$$

q_m = volumetric flow rate per volume of shale matrix element, cm³/sec/cm³

Boundary and initial conditions for an infinite reservoir producing at a constant rate are

$$\Delta p_f = 0, \quad t = 0 \quad ; \quad r_w < r < \infty \quad (9a)$$

$$\Delta p_f = 0, \quad \text{as } r \rightarrow \infty \quad ; \quad t > 0 \quad (9b)$$

$$\left(\frac{\partial p_f}{\partial r} \right)_{r=r_w} = \frac{q \mu}{2\pi r_w k_f h} = \text{constant}, \quad t > 0 \quad (9c)$$

The solution of Eq. 9 depends on the source term q_m , which is the volumetric flux from the surface of

the shale matrix. As mentioned earlier, two types of matrix element will be chosen; i.e., cylindrical and spherical.

The solutions for q_m are developed for both a cylindrical and a spherical element in Appendix A. Substitution of the source term in Eq. 9 in Laplace space yields

$$\frac{1}{r} \frac{\partial}{\partial r} \left(r \frac{\partial \bar{\Delta p}_f}{\partial r} \right) - \frac{s}{\eta(s)} \bar{\Delta p}_f = 0 \quad (10)$$

For cylinders

$$\frac{1}{\eta(s)} = \frac{2k_m}{s a k_f} \lambda \frac{I_1(\lambda a)}{I_0(\lambda a)} + \frac{1}{\eta_f} \quad (11)$$

and for spheres

$$\frac{1}{\eta(s)} = \frac{3}{s k_f} \frac{k_m}{a} \left[\lambda \coth(\lambda a) - \frac{1}{a} \right] + \frac{1}{\eta_f} \quad (12)$$

where

a = radius of the matrix element, cm

$$\lambda^2 = \frac{s}{\eta_m}$$

s = Laplace space variable

Boundary conditions for Eq. 10 become

$$\bar{\Delta p}_f = 0, \text{ as } r \rightarrow \infty \quad (13)$$

$$\left(\frac{\partial \bar{\Delta p}_f}{\partial r} \right)_{r=r_w} = \frac{1}{s} \frac{q\mu}{2\pi r_w h k_f}, \text{ as } r = r_w \quad (14)$$

The solution for Eq. 10 in Laplace space subject to boundary conditions (Eq. 13 and Eq. 14) is¹²

$$\bar{\Delta p}_f = \frac{q\mu}{2\pi r_w h k_f} \frac{\sqrt{\eta(s)}}{s^{3/2}} \frac{K_0 \left[\sqrt{\frac{s}{\eta(s)}} r \right]}{K_1 \left[\sqrt{\frac{s}{\eta(s)}} r_w \right]} \quad (15)$$

Equation 15 gives the Laplace transform of the pressure distribution in an infinite-dual porosity reservoir producing at a constant rate. The exact inversion of Eq. 15 is complicated. Therefore, the pressure can be computed using a numerical Laplace transform inversion technique. The Schapery^{12,18} inversion method with a modification can also be applied to the Laplace transform solution (Eq. 15) in order to get an approximate solution in real space. The result is

$$p_{fD} = \sqrt{\frac{e^{\gamma t} \eta(1/e^{\gamma t})}{r_w^2}} \frac{K_0 \left[r \sqrt{e^{\gamma t} \eta(1/e^{\gamma t})} \right]}{K_1 \left[r_w \sqrt{e^{\gamma t} \eta(1/e^{\gamma t})} \right]} \quad (16)$$

where

$$\gamma = 0.57722 \dots \text{Euler's constant}$$

$$e = 2.7182$$

$$p_{fD} = \frac{2\pi k_f h (p_i - p_f)}{\mu q}$$

$\eta(1/e^{\gamma t})$'s are given by Equations 11 and 12 for cylinders and spheres, respectively, where $s = 1/e^{\gamma t}$.

The solution given by Eq. 16 is a function of the fracture and matrix diffusivities (η_f and η_m), the radius of the matrix element (a), the wellbore radius (r_w), and time (t). Therefore, the dimensionless pressure, p_{fD} , is not the conventional dimensionless pressure as used in petroleum engineering literature. Nevertheless it is not a function of the pressure drop ($p_i - p_f$), the production rate (q) and the formation thickness (h). We can also define the following parameters for simplicity as

$$k_{mD} = \frac{k_m}{a^2}, \text{ darcy/cm}^2$$

$$k_{fD} = \frac{k_f}{r_w^2}, \text{ darcy/cm}^2$$

$$\omega_f = (\phi c \mu)_f, \text{ cp/atm}$$

$$\omega_m = (\phi c \mu)_m, \text{ cp/atm}$$

Equation 16 can be written in terms of these parameters as

$$p_{fD} = \sqrt{e^{\gamma t} \eta(1/e^{\gamma t})} \frac{K_0 \left[r \sqrt{e^{\gamma t} \eta(1/e^{\gamma t})} \right]}{K_1 \left[r_w \sqrt{e^{\gamma t} \eta(1/e^{\gamma t})} \right]} \quad (17)$$

where

$$r_D = \frac{r}{r_w}$$

For cylinders

$$\frac{1}{\eta(1/e^{\gamma t})} = \frac{2\sqrt{e^{\gamma t} k_{mD} \omega_m} I_1 \left(\sqrt{\omega_m / e^{\gamma t} k_{mD}} \right)}{k_{fD} I_0 \left(\sqrt{\omega_m / e^{\gamma t} k_{mD}} \right)} + \frac{\omega_f}{k_{fD}} \quad (18)$$

and for spheres

$$\frac{1}{\eta(1/e^{\gamma t})} = \frac{3e^{\gamma t} k_{mD}}{k_{fD}} \left[\sqrt{\omega_m / e^{\gamma t} k_{mD}} \coth \left(\sqrt{\omega_m / e^{\gamma t} k_{mD}} \right) - 1 \right] + \frac{\omega_f}{k_{fD}} \quad (19)$$

Thus, a fractured reservoir can be characterized in terms of the four basic parameters: k_{mD} , k_{fD} , ω_f , and ω_m .

The interporosity flow parameter, λ_D , is defined by Warren and Root⁴ as

$$\lambda_D = \frac{\alpha k_m r_w^2}{k_f} \quad (20)$$

where

$$\alpha = \text{shape factor}$$

Equation 20 can be approximated for cylinders and spheres as

$$\lambda_D = 128 \frac{k_m}{a^2} \frac{r_w^2}{k_f} \text{ for cylinders}$$

$$\lambda_D = 240 \frac{k_m}{a^2} \frac{r_w^2}{k_f} \text{ for spheres}$$

This study does not indicate that, if λ_D is less than 5×10^{-6} , dual-porosity systems will always show two parallel straight lines. Warren and Root state that as $\lambda_D \rightarrow \infty$, fractured reservoirs will behave as homogeneous ones. Also, if $k_m=0$ then $\lambda_D=0$ and again the system will behave as a homogeneous reservoir.

Long Time Approximations

Case 1: Cylindrical Elements

Let us simplify Eq. 11 for small values of s , which is equivalent to considering a long time. Bessel functions for small values of λ are

$$I_0(\lambda a) = 1, \quad \lambda a < 0.1 \text{ with } 0.25 \text{ percent error} \\ \lambda \rightarrow 0$$

and

$$I_1(\lambda a) = \frac{1}{2} \lambda a, \quad \lambda a < 0.1 \text{ with } 0.006 \text{ percent error} \\ \lambda \rightarrow 0$$

$$\text{where } \lambda^2 = \frac{s}{\eta_m}$$

Substituting these values in Eq. 11 yields

$$\frac{1}{\eta(s)} = \frac{(\phi c)_m \mu + (\phi c)_f \mu}{k_f} \quad (20)$$

The parameter $\eta(s)$ is thus no longer a function of s . The dual-porosity system for long time will behave like a single porosity system. The parameter λa is related to the matrix parameters and time by

$$\lambda a = \sqrt{\frac{1}{2t_{mD}}} < 0.1 \quad (21)$$

where

$$t_{mD} = \frac{k_m t}{(\phi c)_m \mu a^2}$$

A limit can be found directly from inequality 21 as

$$t_{mD} > 50 \quad (22)$$

If t_{mD} is greater than 50 for a given time and matrix parameter, the first straight line (if it exists) from pressure drawdown data will not be seen.

Case 2: Spherical Elements

Equation 12 can be simplified for small values of s as follows:

The hyperbolic function for small values of λ is

$$\coth(\lambda a) = \frac{1}{\lambda a} + \frac{\lambda a}{3}, \quad \lambda a < 0.1 \text{ with } 0.0002 \text{ percent error} \\ \lambda \rightarrow 0 \quad (23)$$

$$\text{where } \lambda^2 = \frac{s}{\eta_m}$$

Substituting Eq. 23 into Eq. 12 yields (as in the cylindrical case) we get

$$\frac{1}{\eta(s)} = \frac{(\phi c)_m \mu + (\phi c)_f \mu}{k_f}$$

If $\lambda a < 0.1$ then the same inequality ($t_{mD} > 50$) can also be found for the spherical case.

DISCUSSION OF RESULTS

Figure 3 presents pressure drawdown data for different models. Kazemi's and Warren and Root's data are reproduced from Figure 6 in Ref. 7. The idealized reservoir parameters are taken from Table 1, Case 1 from Ref. 7 and are presented here in Table 1. Kazemi's model does not have a one-to-one relationship with our model. We have attempted to reproduce his data with some modification of the model. Therefore, an exact comparison of the two results is not expected. As can be seen from Figure 3, when the radius of the matrix element (a) becomes larger the difference between the two results diminishes. For small matrix element radius (a), the drawdown curves do not give two parallel straight lines. However, they displace two straight lines with different slopes. The first straight line will be referred to as early time period which is followed by a transition zone and a late time period. During the late time period (the second straight line) the fractured reservoir behaves like a single porosity system. But the storage of the system will be the sum of the fracture and matrix storages as indicated by Eq. 20.

The curves we have presented do not show a point of inflection which has been customarily used to analyze pressure and buildup and drawdown data.

During the transition period, the Warren and Root model behaves differently than the model presented here. This can also be seen from Figure 2 of Ref. 12.

The choice of element shape makes a little difference during the early time period and the transition time, depending on the size of the element. During the early time period, it is interesting to observe the difference between the cylindrical and spherical solutions for $a = 20$ cm. However, for $a = 1000$ cm the difference in the two solutions appears during the transition period. In fact, when $a = 1000$ cm, Warren and Root, Kazemi, and the results presented here are almost identical during the early time period.

The behavior of a dual porosity system is different than a homogeneous reservoir as can be seen from Fig. 3. However, a dual porosity system does not always displace two parallel straight lines. Figure 4 presents simulated buildup data for an infinite dual porosity reservoir. The Horner plot of this data shows two straight lines with different slopes and a transition period. For a late-time period the slope of the straight lines is equal to 1.151 per log cycle. Thus, the slope is inversely proportional to the fracture permeability. The slope of the first straight line is smaller than the first one and does not yield either the fracture or the matrix permeabilities. More work has to be done to analyze the first straight line.

Figure 5 presents simulated pressure interference data from an observation well at a distance $r_D = 1000$. For the time smaller than 1000 hours, the pressure data can be matched with the exponential integral solution.

If we run the test less than 1000 hours for this particular reservoir, despite the apparent good match, the type-curve matching techniques will yield the fracture permeability but not the fracture porosity, matrix porosity, or the total system porosity ($\phi_m + \phi_f$). For this particular case, $\phi_m = 0.05$, $\phi_f = 0.001$ and the estimated porosity from the match is about 0.017. Figure 6 shows the Horner plot of the buildup data for the same observation well. For the late-time period the slope is only equal to 1.075 per log cycle which is less than 1.151. The permeability calculated from this slope will be greater than the matrix permeability. However, since the difference between the calculated permeability and the fracture permeability is small, this difference is not detected by the type-curve matching in Fig. 5.

The Horner plot of the buildup data does not show a second straight line. As mentioned above, the Horner buildup plot for a producing well for the same reservoir (Fig. 4) shows two straight lines with different slopes.

Figure 7 shows the dimensionless fracture pressure (P_{fD}) for infinite dual-porosity reservoirs producing at a constant rate as a function of logarithm of time for various k_{mD} (k_m/a^2). Curves 1 and 2 do not indicate two straight lines. Curves 3 and 4 both show two straight lines with different slopes. Curve 5 shows two almost parallel straight lines. Thus, two parallel semilog straight lines for fractured reservoirs can only be observed for specific cases. However, dual porosity systems do behave differently from homogeneous (single porosity) systems.

Figure 8 shows the dimensionless fracture pressure as a function of the logarithm of time for various values of $\omega_f[(\phi\mu)_f]$. For this case the interporosity flow parameter (λ_D) is less than 10^{-7} , where:

$$\lambda_D = 128 \frac{k_m r_w^2}{k_f a^2}$$

Except for curve 2, the curves do not display two parallel semilog straight lines. Instead, they display two straight lines with different slopes. Therefore, the interporosity flow parameter (λ_D) is not the only parameter which characterizes the semilog behavior of pressure data from dual porosity reservoirs.

Figures 9 through 12 show some results from the numerical simulator described in Ref. 14. In each case the well was flowed for 4 years at a constant rate of 25 MCFD and then shut-in for 45 days. The first three points obtained after shut-in are not, in general, considered reliable.

Figure 9 shows a Horner buildup plot with a very low value of k_{mD} ($9.29 \cdot 10^{-8}$ md/ft²). We are essentially seeing the first straight line and a small portion of the transition period. The significance of this is that k_{mD} is one of the basic parameters which controls gas production from the shale matrix. The slope of this Horner graph yields lower permeability than input fracture permeability. However, theoretically it should yield higher value than fracture permeability because the effect of the matrix permeability is apparent during the early time period. This difference may be within the error limits of the simulated data and its slope.

Figure 10 shows the Horner plot for the same conditions used in Figure 9 except k_{mD} . In Fig. 10 k_{mD} has been increased to $3.72 \cdot 10^{-6}$ md/ft² by decreasing

the matrix element radius (a) from 1000 cm to 50 cm. Here we see dual porosity effects in the form of two apparent straight line slopes which are approximately parallel and are separated due to a transition period. However, the slopes are not parallel and neither gives exactly the input value of fracture permeability. The first slope is very difficult to get and, by coincidence, gives almost exactly the input value of fracture permeability. The second slope, which should give exactly the input value of k_f , gives a slightly lower value. This could be due to the approximate method of analysis used but is more likely due to the fact that the well was not shut in long enough. That is, the 45-day shut-in only corresponds to a t_{mD} of 5.67 ($t_{mD} < 50$) and hence matrix effects may still be present. The vertical separation is related to the relative storage capacity of the fracture system as compared to the shale matrix.

The buildup shown in Fig. 11 is for the same conditions as in Fig. 10 except that gas slippage has been included according to the relation given by Jones.¹⁷ Note that the first apparent slope gives a higher permeability than the first slope in Fig. 10. This is expected since the effect of gas slippage is to increase the effective gas permeability. However, the second slope is surprisingly low, resulting in an even higher calculated permeability value. Both the duration of the transition zone and the vertical separation are affected by gas slippage.

Figure 12 shows a Horner buildup plot for the conditions of Fig. 11 with desorption included. Since desorption acts as a source term for the shale matrix, one would expect to calculate an even higher permeability than in Fig. 11. This is indeed the case; as shown, a value of 0.119 md was obtained from the first slope. The second slope behaves more as expected in that it gives a permeability value close to the fracture permeability (even though t_{mD} is much less than 50). It should be noted that the transition zone is both longer and flatter than in either Fig. 9 or 10.

These results have not been completely analyzed and are presented here for the first time to show, together with analytical results, the qualitative effects on pressure buildup data of a dual porosity gas flow system with low matrix permeability, gas slippage, and desorption.

CONCLUSIONS

The main purpose of this study was to develop well testing techniques for Devonian shale gas reservoirs by using analytical methods and the numerical simulator.¹⁴ For some sets of reservoir parameters within the limit of the Warren and Root model, we have not observed the characteristic behavior of the fractured reservoirs as presented by Warren and Root. Therefore, we wanted to further investigate to determine whether this is due to very tight nature of Devonian shale reservoirs or an inconsistency in the Warren and Root model. Thus, new approximate analytical solutions were developed for the constant rate case considering cylindrical and spherical matrix elements.

The solutions have been checked with other analytical and numerical solutions for certain cases of the total system studied. Good agreement has been found with these available results. The following conclusions can be drawn from the results of this

study.

1. The Warren and Root model is applicable only for special cases of the fractured reservoir parameters.

2. The interporosity flow parameter (λ_D) is not the only parameter which characterized the nature of the semilog straight lines.

3. We have shown that if the dimensionless time (t_{mD}), which is a function of the matrix parameters, is greater than 50, the dual porosity system will behave like a homogeneous (single porosity) system with storage equal to the total system storage $(\phi)_t = (\phi)_m + (\phi)_f$.

4. For simplicity we have defined four parameters (k_{fD} , k_{mD} , ω_f , and ω_D) which can fully describe the behavior of a fractured reservoir.

5. The type-curve matching techniques may indicate a fracture permeability which is slightly greater than true fracture permeability. Also, the porosity estimated from type-curve matching will indicate a higher value than the fracture porosity and a lower value than the total system porosity. However, this area has to be further investigated to develop methods for estimating fracture and matrix porosity and matrix permeability.

NOMENCLATURE

a	=	radius of shale matrix element, ft (cm)
b	=	Klinkenberg factor, psia (atm)
c	=	concentration of adsorbed gas, mole/cm ³
h	=	formation thickness, ft (cm)
I	=	modified Bessel functions
K	=	modified Bessel functions
k	=	permeability, md (darcy)
k_{fD}	=	$\frac{k_f}{r_w^2}$, md/ft ² (darcy/cm ²)
k_{mD}	=	$\frac{k_m}{a^2}$, md/ft ² (darcy/cm ²)
M	=	molecular weight, lb/mole (g/mole)
p	=	pressure, psia (atm)
q	=	flow rate, bbl/day (cm ³ /sec)
r	=	radial location, ft (cm)
s	=	Laplace space variable
T	=	reservoir temperature, °R (°K)
t_{mD}	=	$\frac{k_m t}{(\phi)_m \mu a^2}$
w	=	mass flow rate per volume of matrix element, g/sec/cm ³
w_d	=	desorption rate, g/sec/cm ³
z	=	real gas deviation factor
α	=	shape factor
ρ	=	density, g/cm ³
μ	=	viscosity, cp
ϕ	=	porosity
η	=	diffusivity (k/φμc)
$\eta(s)$	=	defined by Equations 11 and 12
λ^2	=	$\frac{s}{\eta_m}$
λ_D	=	$\frac{\alpha k_m r_w^2}{k_f}$
γ	=	0.57722..., Euler's constant
ω_f	=	$(\phi\mu)_f$, cp/psi (cp/atm)
ω_m	=	$(\phi\mu)_m$, cp/psi (cp/atm)

Subscripts

f = fracture

D	=	dimensionless
d	=	desorption
g	=	gas
i	=	initial
l	=	liquid
m	=	matrix
t	=	total
w	=	well
0	=	Bessel functions of zero order
1	=	Bessel functions of one order

ACKNOWLEDGEMENT

This work was done in part under Contract No. DE-AT21-78MC08216.

The authors gratefully acknowledge the aid and encouragement given by Mr. Charles A. Komar, Project Manager of the Eastern Gas Shales Project at the U.S. Department of Energy Morgantown Energy Technology Center (METC).

The authors thank the management of Science Applications, Inc., Morgantown, West Virginia, for permission to present this paper.

REFERENCES

- Elkins, L.F.: "Reservoir Performance and Well Spacing, Spraberry Trend Area Field of West Texas", Trans., AIME (1953) 198, 177.
- Pollard, P.: "Evaluation of Acid Treatments from Pressure Build-Up Analysis", Trans., AIME (1959) 216, 38-43.
- Pirson, R.S., and Pirson, S.J.: "An Extension of the Pollard Analysis Method of Well Pressure Build-Up and Drawdown Tests", Paper No. SPE 101 presented at the 36th Annual SPE Fall Meeting, Dallas, Texas, Oct. 8-11, 1961.
- Warren, J.E., and Root, P.J.: "The Behavior of Naturally Fractured Reservoirs", Soc. Pet. Eng. J. (Sept., 1963) 245-255.
- Barenblatt, G.L., and Zheltov, Yu.P.: Soviet Physics, Doklady (1960) 5, 522.
- Odeh, A.S.: "Unsteady-State Behavior of Naturally Fractured Reservoirs", Soc. Pet. Eng. J. (March, 1965) 60-66.
- Kazemi, H.: "Pressure Transient Analysis of Naturally Fractured Reservoirs with Uniform Fracture Distribution," Soc. Pet. Eng. J. (Dec. 1969) 451-458.
- Kazemi, H., Seth, J.S., and Thomas, G.W.: "The Interpretation of Interference Tests in Naturally Fractured Reservoirs with Uniform Fracture Distribution." Soc. Pet. Eng. J. (Dec. 1969) 463-472.
- Crawford, G.E., Hagedorn, A.R., and Pierce, A.E.: "Analysis of Pressure Buildup Tests in Naturally Fractured Reservoir," paper SPE 4558 presented at SPE-AIME 48th Annual Fall Meeting, Las Vegas, Nev., Sept. 30-Oct. 3, 1973.

10. Strobel, C.J., Gulati, M.S., and Ramey, H.J., Jr.: "Reservoir Limit Tests in a Naturally Fractured Reservoir--A Field Case Study Using Type Curves," J. Pet. Tech. (Sept. 1976)
11. de Swaan, O.A.: "Analytic Solutions for Determining Naturally Fractured Reservoir Properties by Well Testing," Soc. Pet. Eng. J. (June 1976) 117-122.
12. Najurieta, H.L.: "A Theory for the Pressure Transient Analysis in Naturally Fractured Reservoirs," paper SPE 6017 presented at the SPE-AIME 51st Annual Fall Technical Conference and Exhibition, New Orleans, La., Oct. 3-6, 1976.
13. Najurieta, H.L.: "Interference and Pulse Testing in Uniformly Fractured Reservoirs," paper SPE 8283 presented at the SPE-AIME 54th Annual Fall Technical Conference and Exhibition, Las Vegas, Nev., Sept. 23-26, 1979.
14. Kucuk, F., and Sawyer, W.K.: "Modeling of Devonian Shale Gas Reservoir Performance," Proceedings of Third Eastern Gas Shales Symposium, Morgantown, WV, Oct. 1-3, 1979.
15. Thomas, J., Jr., and Frost, R.R.: "Internal Surface Area and Porosity in Eastern Gas Shales From the Sorption of Nitrogen, Carbon Dioxide, and Methane," proceedings of First Eastern Gas Shales Symposium, Morgantown, WV, Oct. 17-19, 1977.
16. Klinkenberg, L.J.: "The Permeability of Porous Media to Liquids and Gases," Drilling and Production Practice (1941) 200-213.
17. Jones, F.O., and Owens, W.W.: "A Laboratory Study of Low Permeability Gas Sands", paper SPE 7551 presented at SPE Symposium on Low Permeability Gas Reservoirs, Denver, CO, May 20-22, 1979.
18. Schapery, R.A.: "Approximate Methods of Transformation for Viscoelastic Stress Analysis," Proc., Fourth U.S. National Congress of Applied Mechanics (1961) 1075-1085.

APPENDIX A

Cylindrical Matrix Elements

The flow in the matrix element is given by Eq. 8. Equation 8 can be simplified by using assumptions made earlier in the radial-cylindrical coordinates, as

$$\frac{1}{r} \frac{\partial}{\partial r} \left(r \frac{\partial \Delta p_m}{\partial r} \right) = \frac{1}{\eta_m} \left(\frac{\partial \Delta p_m}{\partial t} \right) \quad (A-1)$$

where

$$\Delta p_m = p_i - p_m$$

$$\eta_m = \frac{k_m}{(\phi c \mu)_m}$$

Boundary and initial conditions for Eq. A-1 are

$$\Delta p_m = 0, \quad t = 0, \quad 0 \leq r \leq a \quad (A-2)$$

$$\Delta p_m = \text{finite, at } r = 0, \quad t < 0 \quad (A-3)$$

$$\Delta p_m = \Delta p_f, \quad \text{at } r = a \quad (\text{at the surface of the matrix element}); \quad t > 0 \quad (A-4)$$

where

$$a = \text{radius of the matrix element}$$

The solution of Eq. A-1 subject to Eqs. A-2 to A-4 in Laplace space is given by

$$\overline{\Delta p_m} = \overline{\Delta p_f} \quad I_0(\lambda r) / I_0(\lambda a) \quad (A-5)$$

where

$$\lambda^2 = \frac{s}{\eta_m}$$

$$s = \text{Laplace space variable}$$

$$I_0, I_1 = \text{Bessel functions}$$

The volumetric flux from the cylindrical surface in Laplace space is given by

$$\overline{q}_m = - \frac{2k_m}{\mu a} \left(\frac{\partial \overline{\Delta p}}{\partial r} \right)_{r=a} \quad (A-6)$$

Taking the derivative of Eq. A-5 with respect to r , and setting r equal to a yields the source term for a cylindrical element as

$$\overline{q}_m = - \frac{2k_m}{\mu a} \lambda \overline{\Delta p_f} \quad I_1(\lambda a) / I_0(\lambda a) \quad (A-7)$$

Spherical Matrix Element

The flow equation for the matrix element is given by Eq. 8 which can be written in spherical coordinates as

$$\frac{1}{r^2} \frac{\partial}{\partial r} \left(r^2 \frac{\partial \Delta p_m}{\partial r} \right) = \frac{1}{\eta_m} \left(\frac{\partial \Delta p_m}{\partial t} \right) \quad (A-8)$$

This equation can be solved using the similar boundary and initial conditions for the cylindrical element case. The solution in Laplace space for a spherical element is

$$\overline{\Delta p_m} = \frac{1}{r} a \overline{\Delta p_f} \frac{\sinh(\lambda r)}{\sinh(\lambda a)} \quad (A-9)$$

and the source term, \overline{q}_m is

$$\overline{q}_m = \frac{3k_m}{a\mu} \overline{\Delta p_f} \left[\lambda \coth(\lambda a) - \frac{1}{a} \right]$$

where

$$\lambda^2 = \frac{s}{\eta_m}$$

$$a = \text{radius of sphere}$$

TABLE 1

FRACTURE PERMEABILITY (k_f)	=	7236.39 md
MATRIX PERMEABILITY (k_m)	=	0.01 md
FRACTURE POROSITY (ϕ_f)	=	0.45 fraction
MATRIX POROSITY (ϕ_m)	=	0.05 fraction
FRACTURE THICKNESS (b)	=	0.025 feet
MATRIX BLOCK THICKNESS (h)	=	9.05 feet
PRODUCTION RATE (q)	=	90.5 barrels/day
VISCOSITY (μ)	=	1.0 cp
COMPRESSIBILITY (c_t)	=	10^{-5} psi ⁻¹

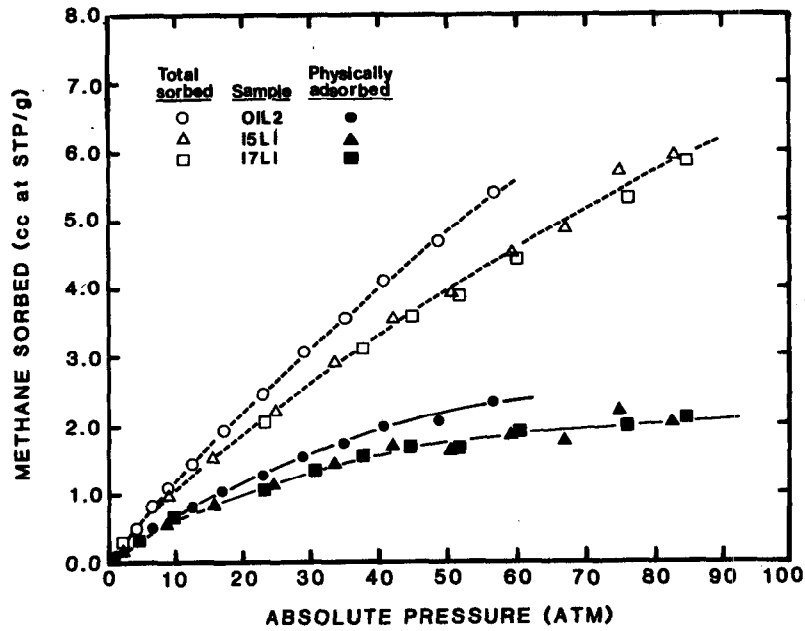


Fig. 1 - Methane sorption Isotherms at 28°C.

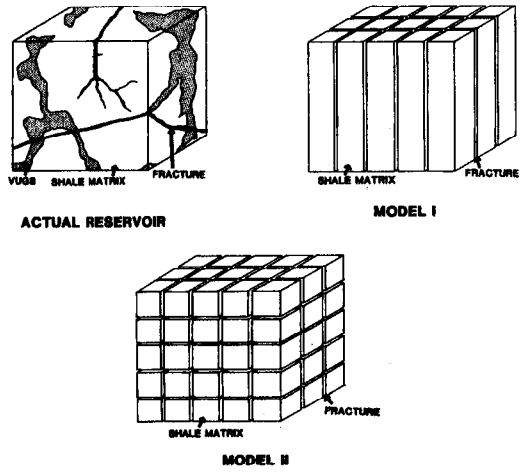


Fig. 2 - Dual porosity models.

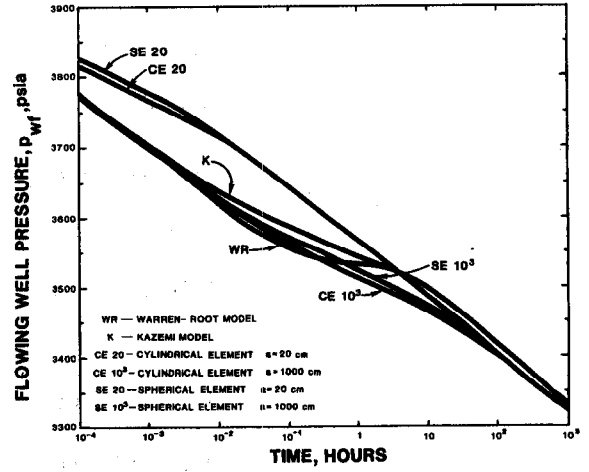


Fig. 3 - Pressure drawdown data from different dual-porosity models.

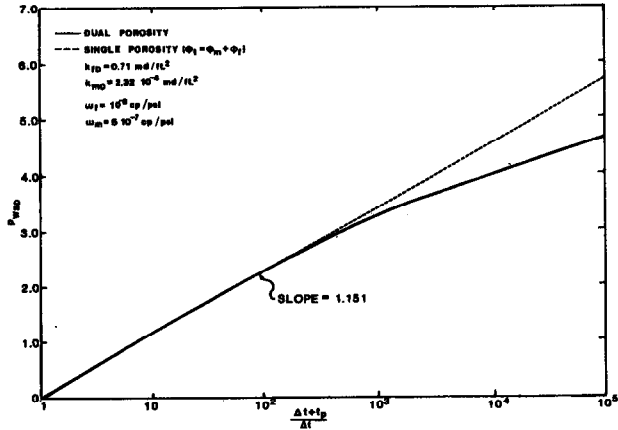


Fig. 4 - Pressure buildup for a dual-porosity model.

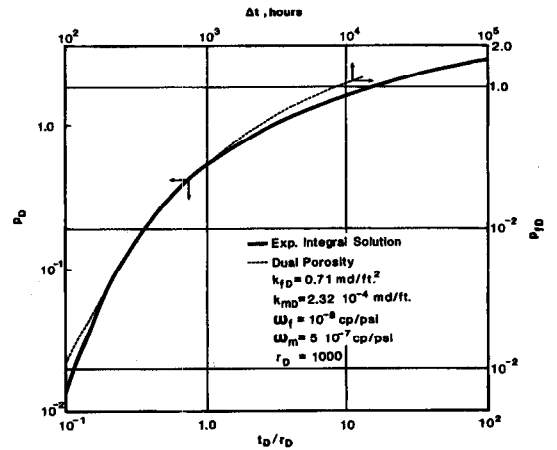


Fig. 5 - Type-curve match for pressure interference data.

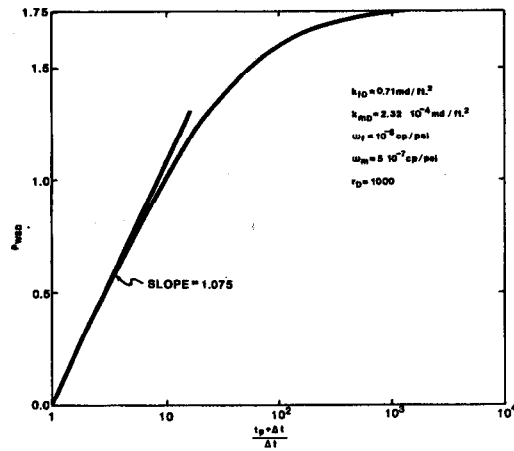


Fig. 6 - Pressure buildup for an observation well.

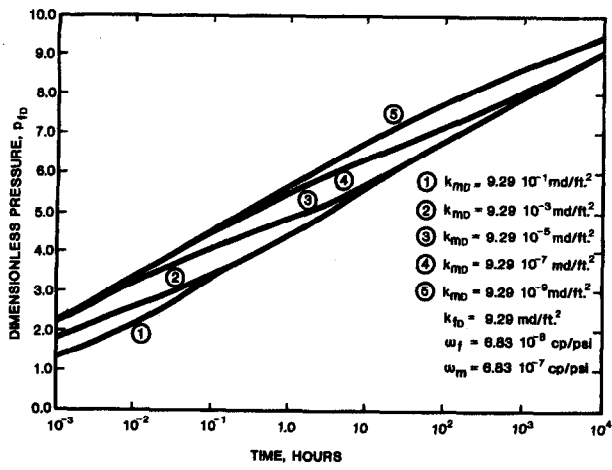


Fig. 7 - Dimensionless pressure as a function of time for various k_{mD} (k_m/a^2).

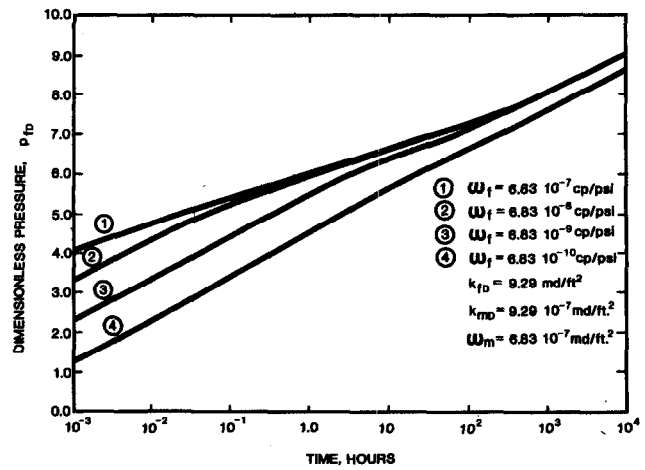


Fig. 8 - Dimensionless pressure as a function of time for various ω_f ($(\phi\mu c)_m$).

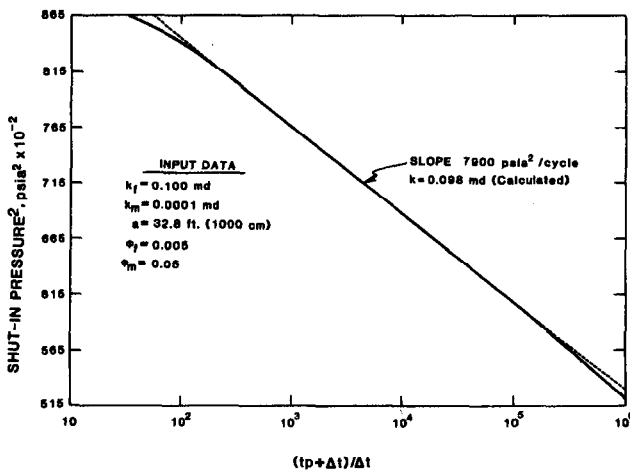


Fig. 9 - Pressure buildup for low value of k_{mD} (k_m/a^2).

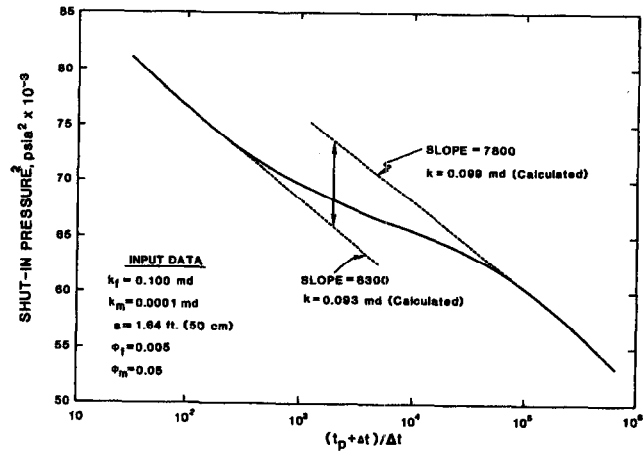


Fig. 10 - Pressure buildup for intermediate value of k_{mD} (k_m/a^2).

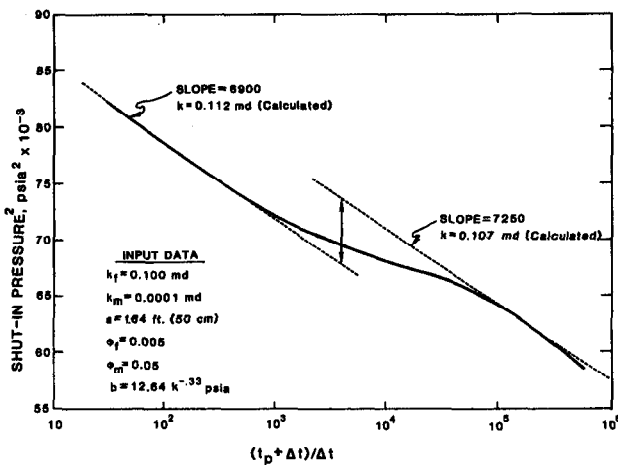


Fig. 11 - Pressure buildup with gas slippage.

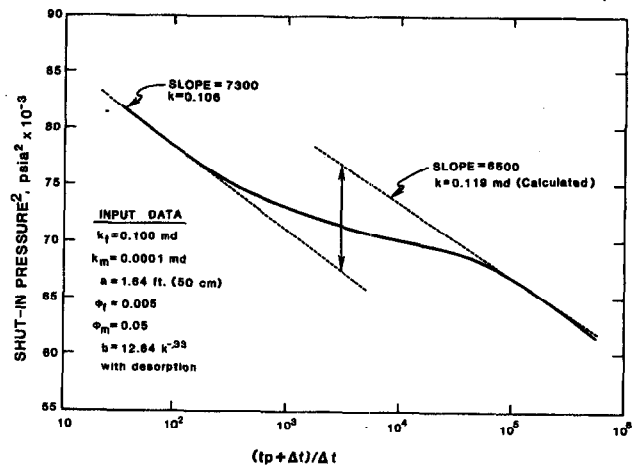


Fig. 12 - Pressure buildup with gas slippage and desorption.